**International Journal of Advanced Engineering Research and Science (IJAERS)**
*Peer-Reviewed Journal*
*ISSN: 2349-6495(P) | 2456-1908(O)*
*Vol-12, Issue-7; Jul, 2025*
**Journal Home Page Available:** https://ijaers.com/
**Article DOI:** https://dx.doi.org/10.22161/ijaers.127.1

# Effect of $Fe_2O_3$ additives on the sintering mechanism of a high strength ceramsite from a CFB fly ash

Ikechukwu Okeke, Peng Liyang, Yuhong Qin*, Chukwubuike Chiemerie Onwuagbu, Afreh Paul, Maywish Islam

College of Environment and Ecology, Taiyuan University of Technology, Taiyuan, Shanxi Province, China.
*Corresponding Author

Received: 27 May 2025,

Received in revised form: 25 Jun 2025,

Accepted: 28 Jun 2025,

Available online: 03 Jul 2025

***Keywords*— CFB fly ash, $Fe_2O_3$, ceramsite, sintering mechanism, liquid-phase sintering, compressive strength**

***Abstract*— *The sustainable reutilization of industrial solid waste offers a viable strategy to address environmental concerns associated with coal-fired power generation. This study investigates the role of $Fe_2O_3$ additives in enhancing the sintering behavior, microstructural evolution, and structural properties of high-strength ceramsite synthesized from circulating fluidized bed (CFB) fly ash. A series of ceramsite samples with varying $Fe_2O_3$ contents (0–15 wt%) were sintered at temperatures ranging from 1150°C to 1300°C to evaluate the influence of $Fe_2O_3$ on material performance. The results revealed that the addition of 5 – 10 wt% $Fe_2O_3$ at 1300°C produced optimal results. Microstructural analyses using X-ray diffraction (XRD), scanning electron microscopy (SEM), and thermogravimetric–differential scanning calorimetry coupled with Fourier-transform infrared spectroscopy (TG-DSC-FTIR) demonstrated that $Fe_2O_3$ effectively promotes liquid-phase sintering, facilitates mullite crystallization, and improves particle bonding and densification, while simultaneously moderating gas evolution. However, excessive $Fe_2O_3$ content (>10 wt%) led to reduced strength and densification due to increased porosity and decreased liquid-phase viscosity. This research not only highlights the dual function of $Fe_2O_3$ as both a fluxing and structural stabilizing agent but also provides a practical route for converting coal-based solid waste into high-performance construction materials. The findings contribute to the advancement of sustainable building technologies and support circular economy goals through efficient resource recovery and waste minimization.***

## I. INTRODUCTION

When coal is burned in a circulating fluidized bed combustion (CFBC) boiler, it produces circulating fluidized bed (CFB) fly ash that is significantly different from traditional pulverized fuel combustion fly ash. This is as a result of different combustion conditions which produce fly ash with different mineralogic composition, chemical properties, and structure, which ultimately not only makes CFB fly ash less desirable to use, it also makes it more difficult to use compared to pulverized fly ash [1], [2], With China producing approximately 80–150 million tonnes of CFB fly ash every year, there is a growing need to consider more effective ways to reuse as much CFB fly ash as possible [3]. The physical properties of CFB fly ash do not help its case for use. Unlike pulverized fly ash, many of the CFB fly ash have a distinctly irregular shapes, either blocky or rod-like, along with a very rough, porous, and loosely-bound surface. These characteristics are simply caused by the lack of sufficient liquid phase at combustion temperatures (850–900°C) at which CFB ash is burning, with resulting in lower densities and items having a rougher texture [4]. Additionally, during its cooling, the particles do not form the smooth and spherical glass structures typically formed in other fly ashes. The thermal decomposition of limestone and release of the $CO_2$ upon combustion contribute to the loose and porous nature of CFB fly ash [5], [6]. Qian et al. [7] propose that as anhydrite and clay minerals decrease in proportion, the particles are even more loosely structured. In order to address expansion problems, research has examined processing CFB fly ash into highly porous materials, and it has even been used as an expanding agent in self-leveling mortar [2]. CFB fly ash is also being adopted for various other industries such as binder production, construction materials, road infrastructure, and sulfate activation to contribute to sustainability development [8], [9], [10].

Ceramsite is a construction material that possesses good mechanical resistance in both acidic and alkaline environments, high strength, and high-performing thermal insulation properties [11]. Based on composition ($Fe_2O_3$, $Al_2O_3$, $SiO_2$), ceramsite also shows potential as an effective medium for filtration in industrial wastewater and municipal wastewater treatment systems. Ceramsite is a major component of the construction industry as it is used in making bricks, aggregates for concrete and ceramic-based products [12]. Due to both stability and if being lightweight with high insulation properties, ceramsite has useful applications in a broad spectrum of industries including agriculture, metallurgy, construction and chemical manufacturing [13]. Amid the growing demand for sustainable waste management, research efforts are focused on investigating solid waste-derived materials in the production of high-strength ceramsite. Potential raw materials that have been explored include fly ash, incineration fly ash [14], [15], river sediments [16], industrial tailings [17], sludge [18], [19] coal gangue, red mud, and electrolytic manganese slag [20]. The interest in solid waste recycling is increasingly important to this research avenue [21]. High-strength ceramsite is an artificial lightweight aggregate that is known for its load-bearing capacity, with a cylindrical compressive strength greater than 4.0 MPa and stacking density of 500 to 1200 $kg/m^3$. It is made through a multi-step process which entails: raw material preparation, granulation, and sintering at high temperatures [22], [23]. In the latter, CFB fly ash serves several important purposes, such as to provide $SiO_2$ and $Al_2O_3$, which make up the structure, to add CaO, MgO, and $Fe_2O_3$, which are fluxing agents to aid sintering, and to add C and $CaCO_3$, which act as gas-forming agents to produce porosity and lightweight aggregate [24].

Sintering is an important process to treat fly ash. Fly ash is mixed with silica-alumina materials and fluxing agents to partial melting of the material in the kiln at fixed high temperatures, then, is cooled to solidify. This high-temperature treatment is necessary to detoxify organic contaminants such as dioxins while binding heavy metals, which increases environmental safety of materials made from fly ash [15], [25]. The sintering procedure applied to fly ash shares many similarities with the method used in ceramsite production [26]. The high-temperature treatment of sintering limits the leaching of ion exchange with ceramsite and provides chemical stability to the ceramsite which makes it suitable in encapsulating heavy metals [27]. Therefore, ceramsite made from fly ash by sintering will always show great stability and durability while eliminating leaching and maintaining environmental safety, making them suitable in all construction applications.

However, sintering inevitably generates emissions of harmful gases such as $SO_2$, $NO_x$, and CO. Research by Liu et al. [27] indicates that $SO_2$ is the most significant sulfur-based pollutant released in this process, with approximately 50% originating from the reduction of calcium and magnesium sulfates and another 40% from the combustion of organic sulfur compounds and sulfite decomposition. The degree to which these emissions occur depends on factors such as the sintering atmosphere, airflow, and water vapor levels. Yu et al. [14] examined the influence of sintering temperature and additives on $Al_2O_3$ ceramics, identifying that refining the sintering conditions increases the relative density and the mechanical strength. The basic oxides, $Fe_2O_3$, CaO, or MgO, included or added, amplify the accumulation of crystals and liquid phase that are needed to increase the property of the sintered ceramsite. Similarly, Ma et al. [28] studied the production of ceramic foams by adding 8 wt% of MgO when investigating $Al_2O_3$ ceramics with varied levels of flux and sintering temperature which ultimately lead to increased compressive strength.

The production of alumina creates red mud, which is a significant waste by-product. Red mud has a high concentration of $Fe_2O_3$. According to Wang et al. [29], $Fe_2O_3$ was the most abundant mineral compound in red mud, which comprised of 59.37% of the red mud components. Due to the high concentration of iron, black cores develop, and inter-particle adhesion is limited during ceramsite formation, which can have a great deal of impact on the structure overall [30]. Pei et al. [31] examined the incorporation of red mud in combination with various materials to produce ultra-lightweight ceramsite, finding that $Fe_2O_3$ accounted for approximately 53.96% of the red mud mass. Their results also indicated that as red mud content increased, the bulk density of ceramsite decreased initially but increased thereafter, indicating a complex interaction between additive content and density.

Mi et al. [32] conducted a similar study in which they used both fly ash and red mud as raw materials to produce high strength ceramsite. In the study, the authors examined the ratios of raw materials and sintering conditions. It is reported that the best composition produced a ceramsite with a compressive strength of 21.01 MPa. Mi et al. [32] reported an increase in $Fe_2O_3$ resulted in a ceramsite with a higher density and burned at a lower sintering temperature. The best outcome was $Fe_2O_3$ content of approximately 6-8% as the overall trends observed were porosity, and general strength of the ceramsite improved with increasing sintering temperature. Zou et al. [33] confirmed this observation, stating that to achieve optimum mechanical performance of sintered ceramsite, raw material $Fe_2O_3$ concentrations were held at about 5% to 8%. Taken together, the studies have established the functional significance of $Fe_2O_3$ in CFB fly ash. In addition, the amount of $Fe_2O_3$ content was determined to only affect the initial conditions of the sintering process for producing high-strength ceramsite.

This study aimed to investigate the effect of sintering temperature and $Fe_2O_3$ concentration on the formation and properties of ceramsite. With CFB fly ash serving as the primary raw material, $Fe_2O_3$ was introduced as a flux to improve the sintering process. The research evaluated fundamental physical attributes, including compressive strength, apparent density, stacking density, and water absorption. To obtain a detailed perspective on the sintering process, advanced in situ high-temperature observation methods were employed alongside XRD, TG-DSC-FTIR, and SEM analyses. A key focus was understanding how $Fe_2O_3$ contributes to phase transitions, microstructural evolution, and the final performance of high-strength CFB fly ash ceramsite.

## II. MATERIALS AND METHOD

### 2.1 Raw materials

This research utilized $Fe_2O_3$ and CFB fly ash as raw materials, with the CFB fly ash sourced from Shanxi Pingshuo Gangue Power Generation Co., Ltd., a major coal-based solid waste processing and power generation enterprise in Shanxi Province, China. The $Fe_2O_3$ additive, obtained from Taiyuan Biochemical Technology Co., Ltd., had a purity of over 98%, ensuring its suitability for precise experimental analysis. To determine the chemical composition of the CFB fly ash, X-ray fluorescence spectrometry (XRF) was performed in accordance with the GB/T 176–2017 standard, requiring the sample to be heated to 950°C for 60 min [22]. Loss on ignition (LOI) was also analyzed, with results summarized in Table 1. The XRF analysis showed that $SiO_2$ and $Al_2O_3$ were the dominant oxides, comprising 87.77% of the material, while $Fe_2O_3$, CaO, MgO, $Na_2O$, and $K_2O$ accounted for 7.25%. These values confirm that CFB fly ash meets the chemical criteria for ceramsite production [23]. To further examine its mineral structure, X-ray diffraction (XRD) analysis was conducted. As presented in Fig. 1, kyanite, quartz, and hematite were identified as the primary mineral phases, with anhydrite and lime appearing in smaller amounts. These findings offers an important insight into the mineral composition and structural properties of CFB fly ash.

*Table 1. Chemical composition of the CFB fly ash*

| | Component; wt.% | | | | | | | | | | | | |
|---|---|---|---|---|---|---|---|---|---|---|---|---|---|
| Sample | $SiO_2$ | $Al_2O_3$ | CaO | $Fe_2O_3$ | $TiO_2$ | $K_2O$ | $Na_2O$ | MgO | $SO_3$ | LOI | $SiO_2$ | $Al_2O_3$ | CaO |
| CFB fly ash | 46.47 | 41.30 | 2.63 | 3.46 | 1.85 | 0.73 | 0.08 | 0.35 | 0.36 | 2.53 | 46.47 | 41.30 | 2.63 |

### 2.2 Preparation of ceramsite

This study systematically examined the impact of $Fe_2O_3$ on the physical and chemical properties of ceramsite by preparing 28 different sample sets using CFB fly ash and $Fe_2O_3$ under controlled conditions. The primary objective was to assess the role of $Fe_2O_3$ in enhancing ceramsite strength. The experimental design incorporated $Fe_2O_3$ at four different weight percentages (0 wt%, 5 wt%, 10 wt%, and 15 wt%), while sintering temperatures were set at seven levels: 1150°C, 1175°C, 1200°C, 1225°C, 1250°C, 1275°C, and 1300°C.

To ensure experimental consistency, the CFB fly ash was first dried at 105°C for 24 hours until it reached a stable weight. The dried material was then sieved through a 96 μm (160 mesh) square sieve to achieve uniformity in particle size. The required proportions of CFB fly ash and $Fe_2O_3$ were mixed using a cement mortar mixer, ensuring thorough homogenization before pelletization.

The formation of ceramic pellets (5–10 mm in diameter) was conducted using disc-pelletizing equipment, where the material mixture was combined with a small quantity of water and rotated at a speed of 20–50 r/min to achieve uniform granulation. Sintering was performed in a

KSL-1400X resistance furnace under a precisely controlled heating program. To prevent material cracking due to rapid temperature fluctuations, a 20-minute preheating step was introduced to facilitate gas release. The temperature was then gradually increased to 800°C at a rate of 5°C/min before reaching the final sintering temperature, which was maintained for 60 minutes. Following sintering, the ceramsite samples were allowed to cool naturally inside the furnace until they reached 25°C before being collected for further evaluation

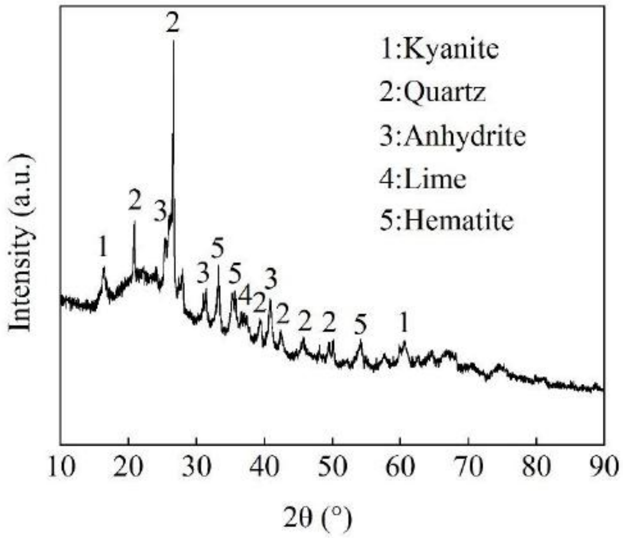

*Fig. 1. XRD analysis of the CFB fly ash*

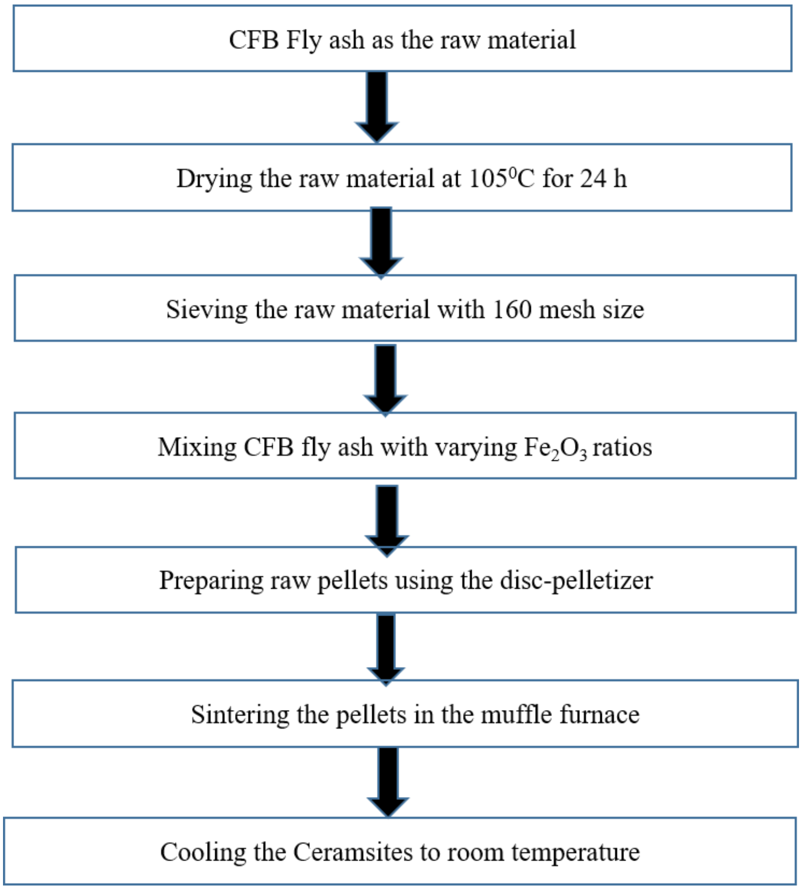

*Fig 2. Flow chart showing the process of producing ceramsite*

### 2.3 Evaluation of physical and chemical properties of ceramsite.

The mineral compositions of both CFB fly ash and sintered ceramsite were examined using X-ray diffraction (XRD). Prior to analysis, the ceramsite samples were crushed and finely ground until they could pass through a 45 µm square sieve.

To evaluate the physical properties of ceramsite, important parameters including apparent density, stacking density, one-hour water absorption, and cylindrical compressive strength were measured following the GB/T17431.2-2010 standard [34]. Due to the large number of ceramsite samples required for the cylindrical compressive strength test, manual pelletizing was not feasible. Instead, a computerized press (HYD-500KG, Dongguan Hongjin Testing Instrument Co., Ltd., China) was used to assess the failure load, which represents the maximum pressure at which the ceramsite sample breaks [34]. The compressive strength was then obtained by calculating the average failure load of twenty ceramsites using Eq. (1) [35], [36].

$$P = \frac{2.8P_c}{\pi X^2} \qquad (1)$$

In this case, P stands for compression strength (MPa), X for ceramsite diameter (mm), and Pc for ceramsite rupture load (N).

The samples' apparent density, stacking density, and water absorption were measured using Eqs. (2), (3), and (4), respectively [34]. To improve the reliability of the data, each sample was tested twice, ensuring greater statistical accuracy.

$$\rho_{ap} = \frac{M1 \times 1000}{V1 - V0 - 500} \qquad (2)$$

where $\rho_{ap}$ stands for the apparent density measured in (kg/m3), m1 stands for the mass of the dried sample measured in (g), V1 is the total volume of the sample, circular metal plate, or water and is measured in (mL), while V0 stands for the volume of the circular metal plate measured in (mL).

$$\rho_{bu} = \frac{(M_2 - M3) \times 1000}{V2} \qquad (3)$$

In this equation, $\rho_{bu}$ stands for the stacking density measured in (kg/m3), and then $m_2$ is the total mass of the sample and measuring cylinder measured in (g), while m3 is the mass of the measuring cylinder (g), and $V_2$ is the volume of the measuring cylinder (ml).

The ratio of water absorption of the ceramsite after immersion in water for 1 h was calculated using Eq. (4):

$$\omega_a = \frac{m_0 - m_1}{m_1} \times 100\% \qquad (4)$$

Where $\omega_a$ stands for 1-h water absorption of ceramsite calculated in %, $m_0$ is the mass of the sample after water absorption, while $m_1$ is the mass of the sample before absorption.

### 2.4 In situ analysis of the macroscopic morphology

Figure 3 illustrates the setup of the in situ high-temperature observation system, which includes a high-temperature furnace, a gas management system, and an image acquisition and processing unit. During the heating process, the morphology of the ceramsite was analyzed using ImageJ 1.46r software. The furnace used in the experiment was almost identical to the one utilized for ceramsite production.

To ensure a controlled environment, nitrogen gas ($N_2$) was introduced at a flow rate of 80 mL/min. This helped remove gases released during sintering while also cooling the quartz observation window. Image acquisition was conducted systematically: during the 30-minute constant temperature phase, images were captured every 10 minutes, and throughout the heating phase, images were taken at 10°C increments from 800°C to 1300°C. The estimated ceramsite area was analyzed using ImageJ 1.46r, and the shrinkage or expansion ratio was calculated based on Equation (5).

$$\frac{Shrinkage}{Expansion(\%)} = \frac{S_t - S_0}{S_0} \times 100\% \qquad (5)$$

Where shrinkage or expansion is defined as the percentage change in the ceramsite's projected area, the ceramsite's projected area at a specific temperature, and the ceramsite's original projected area, mm$^2$.

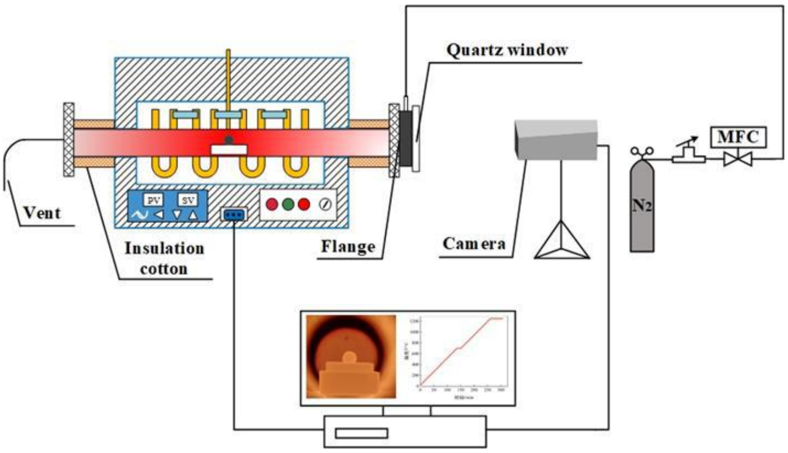

*Fig. 3. An in situ observation instrument*

## III. RESULTS AND DISCUSSION

3.1. The effect of sintering temperature and $Fe_2O_3$ addition on ceramsite properties

The preparation of ceramsite is influenced by four key sintering parameters: sintering temperature, sintering time, preheating temperature [37], and preheating time [38]. Among these, sintering temperature is particularly important and must be carefully managed. If the temperature is too high, an excessive liquid phase forms, which can weaken the ceramsite structure and cause particles to adhere to one another. Conversely, a temperature that is too low results in insufficient liquid phase formation, preventing proper densification.

The impact of $Fe_2O_3$ addition on ceramsite compressive strength at varying sintering temperatures is depicted in Fig. 4. As shown, the compressive strength of ceramsite increased with rising sintering temperatures.

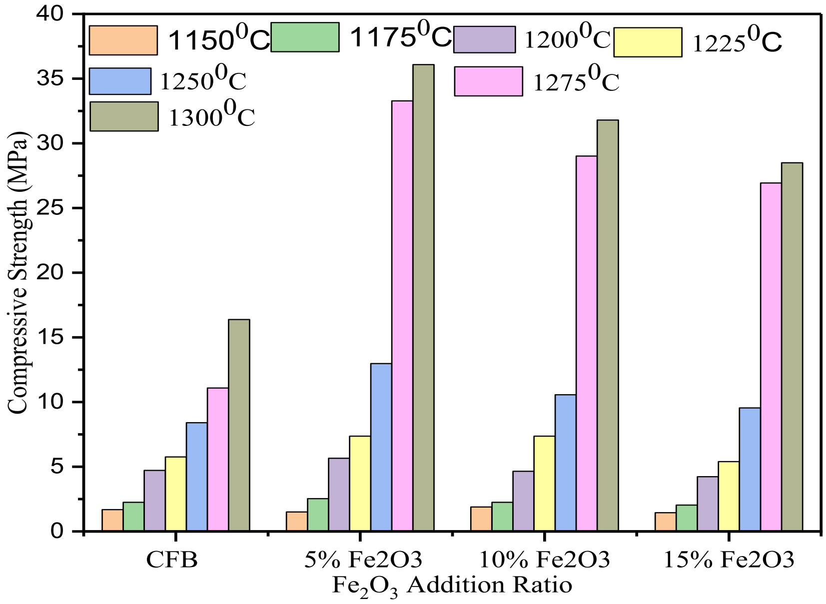

*Fig. 4. Ceramsite's compressive strength with varying $Fe_2O_3$ additive ratios*

The temperature at which ceramsite undergoes sintering has a significant impact on its compressive strength [32]. The data show that increasing the sintering temperature led to a steady rise in strength across all $Fe_2O_3$ additions. However, at 1150°C, the compressive strength remained low, ranging from 1.45 MPa to 1.89 MPa. This was primarily due to insufficient sintering, as the particles had only just started to bond, resulting in weak structural cohesion. At 1175°C, the compressive strength improved noticeably, particularly with $Fe_2O_3$ additions from 5 wt% to 15 wt%. However, the strength still did not reach the 4 MPa requirement outlined in the Chinese National Standard

(GB/T 17431.1–2010) and the Chinese Engineering Construction Standard (T/CECS 10113–2020) [22], [23]. This was mainly due to the low silica-to-aluminum ($SiO_2/Al_2O_3$) ratio in CFB fly ash, which was below 1.5. Additionally, minerals such as mullite, anorthite, and corundum were difficult to melt at this temperature [39]. As a result, the ceramsite lacked sufficient liquid phase formation, which is necessary for effective particle bonding and the development of a strong crystalline structure.

The sintering temperature and $Fe_2O_3$ additives have a major impact on compressive strength. At all temperatures, the control sample containing 0 wt% $Fe_2O_3$ performed the worst. Its strength increased only moderately at higher temperatures, reaching 11.09 MPa at 1275°C and beyond, and was negligible at lower temperatures, ranging from 1.69 to 4.72 MPa at 1150–1200°C. Due to the lack of a fluxing agent, this suggests weak particle bonding and low densification. The 10 wt% $Fe_2O_3$ sample was significantly stronger compared to the sample without $Fe_2O_3$ additives, reaching 29.02 MPa at 1275°C and increasing to 31.80 MPa at 1300°C. Notably, the 15 wt% $Fe_2O_3$ sample reach a peak of 28.49 MPa at 1300°C. However, do not reach the strength of the 5 wt% $Fe_2O_3$ sample, demonstrating that strength is not always improved by increasing $Fe_2O_3$ ratios. The best performance was observed at 1300°C with a 5 wt% $Fe_2O_3$ addition, achieving a compressive strength of 36.09 MPa.

When $Fe_2O_3$ content exceeded 5 wt%, the reduction in liquid phase viscosity negatively affected internal gas discharge and pore formation [31]. However, the addition of $Fe_2O_3$ enhanced the fluxing properties of the raw material, facilitating liquid phase formation and supporting the development of the $Fe_2O_3$–$Al_2O_3$–$SiO_2$ oxide system within the ceramsite. During sintering, the solid particles became more compact and recrystallized, which contributed to the overall increase in ceramsite's compressive strength [40]. The physical properties of ceramsite—such as water absorption, apparent density, and stacking density are closely tied to its strength and are influenced by factors like mineral composition and pore structure.

Figure 5 demonstrates how $Fe_2O_3$ content influences the physical properties of ceramsite at a sintering temperature of 1250°C. The sample containing 5 wt% $Fe_2O_3$ achieved the highest values for stacking density (944.55 kg/m$^3$) and apparent density (1890.68 kg/m$^3$), while maintaining a relatively low water absorption rate of 6.50%. Conversely, the sample with 15 wt% $Fe_2O_3$ at the same temperature exhibited slightly lower stacking and apparent densities of 936.67 kg/m$^3$ and 1764 kg/m$^3$, respectively, and a higher water absorption rate of 8.08%. These findings suggest that the 5 wt% $Fe_2O_3$ addition significantly enhanced ceramsite densification, which is essential for improving its overall strength.

The significant enhancement in compressive strength can be attributed to the closure of pre-existing pores, which restricted moisture movement and improved the material's overall densification. However, the slight increase in water absorption in the 15 wt% $Fe_2O_3$ sample suggests that an excess of $Fe_2O_3$ may lead to non-uniform densification. This is likely due to overfluxing, which facilitates the formation of isolated pores, thereby reducing the effectiveness of the densification process. Ceramsites that are denser and have fewer pores are more effective and help harmful substances solidify [39], [40].

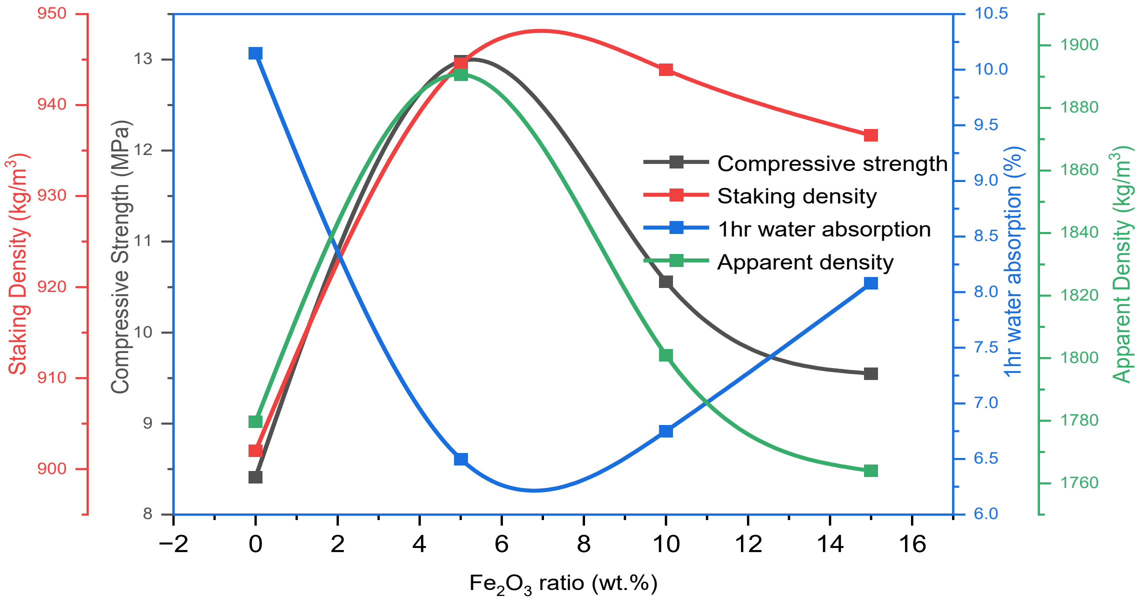

*Fig. 5. Impact of $Fe_2O_3$ addition on ceramsite performance*

At 5 wt% $Fe_2O_3$ addition and a sintering temperature of 1225°C, the ceramsite exhibited improved physical properties, with compressive strength rising to 7.36 MPa, water absorption measured at 12.20%, bulk density at 863.94 kg/m³, and apparent density at 1770.23 kg/m³. As the sintering temperature increased to 1300°C, the ceramsite's surface darkened, and a thick, enamel-like layer formed. Under these conditions, compressive strength peaked at 36.09 MPa, water absorption decreased significantly to 0.19%, bulk density rose to 1189.3 kg/m³, and apparent density reached 2327.85 kg/m³. These enhancements occurred due to a dynamic equilibrium between gas pressure, viscosity, and surface tension of the liquid phase, which facilitated a well-distributed pore structure and increased strength [41], [42].

### 3.2 Macroscopic morphology analysis

High-strength ceramsite is produced from CFB fly ash via high-temperature sintering. During this process, the raw pellets experience expansion and contraction, reflecting the interplay of gas, liquid, and solid phases in ceramsite formation [41], [43]. By monitoring these changes and calculating the projected area variation using Equation (5), the morphological evolution of ceramsite with different $Fe_2O_3$ additions was analyzed.

At lower temperatures, as illustrated in Fig. 6, the projected area remained relatively unchanged regardless of $Fe_2O_3$ concentration. This is due to limited mass transfer and a weak sintering driving force between CFB fly ash particles, indicating that solid-state sintering was predominant [44], [45]. However, as the temperature and holding time increased, the ceramsite entered liquid-phase sintering, leading to a significant reduction in its projected area. The shrinkage intensified with rising temperature, highlighting the dominant role of the liquid phase in shaping the final structure.

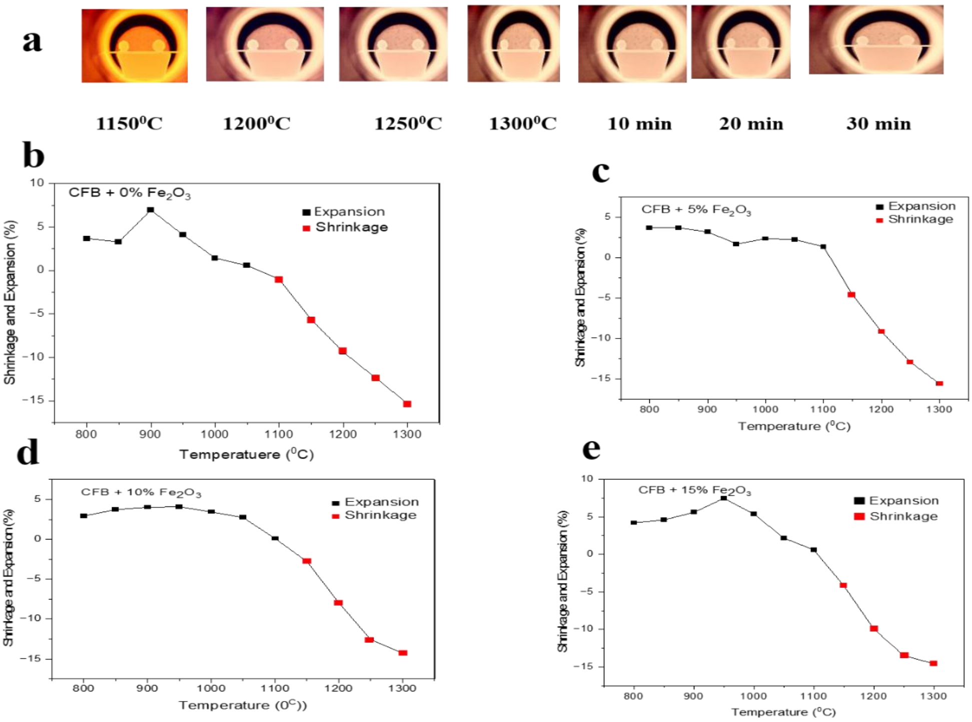

*Fig. 6.Solid-liquid sintering of ceramsite at 1300 °C with varying ratios of $Fe_2O_3$ addition*

### 3.3 Effect of $Fe_2O_3$ on the Shrinkage and Expansion Behavior of Ceramsite during Sintering

The sintering process has a significant impact on ceramsite's final characteristics, particularly its expansion and shrinkage. The addition of $Fe_2O_3$ changes these characteristics and affects the material's structural stability and strength. The ceramsite sample containing 0 wt% $Fe_2O_3$ exhibited the most uncontrolled expansion at 900°C, reaching 6.95%. This behavior suggests significant gas retention in the material because there is no fluxing agent to regulate the bloating process. At 1100°C, however, the sample started to shrink (-1.01%). The sintering driving force was insufficient at temperatures below 1100 °C, and the breakdown of carbonates and other materials, along with the combustion of remaining carbon, only slightly expanded the material. This expansion dropped as the temperature increased. According to Table 1, the loss on ignition (LOI) of CFB fly ash was relatively low at 2.53%, primarily due to the burning of residual carbon. When the temperature remained below 1100°C, this combustion did not generate enough heat to melt minerals such as mullite, corundum, and anorthite, resulting in minimal expansion of the ceramsite. As the temperature rose above 1100°C, liquid-phase sintering took over, leading to continuous shrinkage as the liquid-phase content increased. By 1250°C, the sample had shrunk by 12.34%, and at 1300°C, shrinkage reached 15.29%. These findings suggest that, without $Fe_2O_3$, ceramsite lacks the necessary structural control, causing excessive shrinkage during densification.

The expansion phase improved when 5 wt% $Fe_2O_3$ was added; at 850°C, the maximum expansion was 3.69%. $Fe_2O_3$ acts as a stabilizing agent, preventing excessive bloating, as observed in this sample compared with the 0 wt% $Fe_2O_3$ sample. The decrease started at 1150°C (-4.59%), and it increased at 1250°C (-12.92%). At 1300°C, the sample showed the greatest shrinkage of any composition at -15.58%. The results suggest that $Fe_2O_3$ addition had a significant impact on ceramsite sintering, accelerating the process and reducing the temperature range required for stable shrinkage. Within the optimal temperature range, the formation of an abundant liquid phase contributed to improved compressive strength. The shrinkage rate of the ceramsite's projected area was measured from the initial sintering temperature (Tis) to the end of the heating process. The results showed that when $Fe_2O_3$ was added at 0 wt%, 5 wt%, 10 wt%, and 15 wt%, the shrinkage rates were 15.29%, 15.58%, 14.29%, and 14.56%, respectively, indicating an initial increase followed by a decline. However, at $Fe_2O_3$ levels of 10 wt% and 15 wt%, shrinkage rates declined to 14.29% and 14.56%, respectively. This suggests that excessive $Fe_2O_3$ reduced the viscosity of the liquid phase, affecting the development of the pore structure [46], thereby limiting densification and weakening compressive strength. The slight increase in shrinkage from 15.29% (0 wt% $Fe_2O_3$) to 15.58% (5 wt% $Fe_2O_3$) can be attributed to the reaction of $Fe_2O_3$ with $SiO_2$ and $Al_2O_3$ in CFB fly ash at high temperatures. This reaction facilitated the formation of a low-melting liquid phase, which filled gaps between unmelted particles and promoted densification. The reduction in unmelted solid particles, combined with surface tension effects, helped improve the material's density and compressive strength while decreasing porosity [47].

### 3.4 Effect of crystalline phase on compressive strength

The influence of sintering temperature and $Fe_2O_3$ concentration on ceramsite formation was analyzed using X-ray diffraction (XRD) at varying temperatures and $Fe_2O_3$ levels. Specifically, the ceramsite's composition and mineral phase distribution were examined with 5 wt% $Fe_2O_3$. As presented Figure 7 and Table 2, the primary crystalline phases identified included mullite, cristobalite, anorthite, pyroxene, magnetite, hercynite, and a minor fraction of fayalite. The results indicate that ceramsite's mineral phase composition undergoes significant changes as the sintering temperature increases from 1150°C to 1300°C.

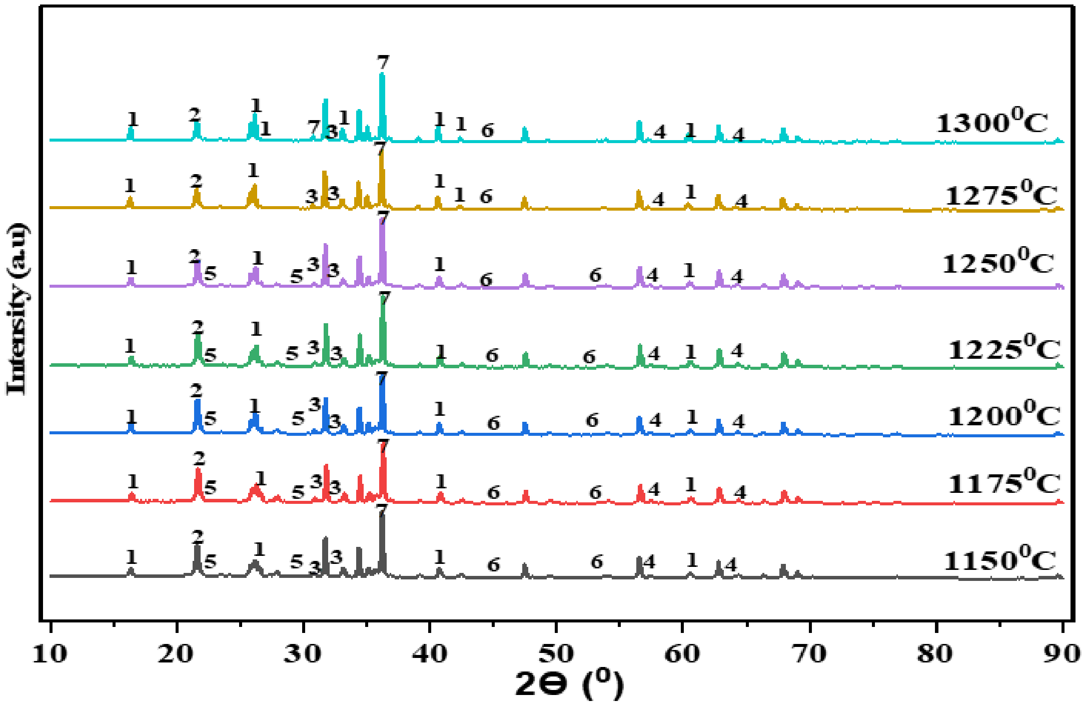

*Fig. 7. XRD analyses of ceramsite with 5 wt% $Fe_2O_3$ at varying sintering temperatures*

1-Mullite ($3Al_2O_3 \cdot 2SiO_2$); 2- Cristobalite ($SiO_2$); 3-Pyroxene $Ca(Mg,Fe)Si_2O_6$, 4-Magnetite ($Fe_3O_4$); 5-Anorthite ($CaAl_2Si_2O_8$); 6 Fayalite ($Fe_2SiO_4$); 7-Hercynite ($FeAl_2O_4$)

XRD analysis revealed a progressive increase in the formation of mullite, hercynite, and pyroxene-type silicates with rising temperature. Mullite began forming at 1150°C and increased significantly between 1200°C and 1275°C, showing sustained intensity at 1300°C. It is the primary phase contributing to high compressive strength due to its interlocking, needle-like microstructure. Hercynite emerged at ≥1150°C as a spinel product of $Fe_2O_3$ and $Al_2O_3$ interaction, playing a role in microstructural densification and thermal stability. Pyroxene phases appeared from 1200°C, contributing to compactness and moderate strength improvement. In contrast, fayalite, a weaker phase with lower hardness, appeared transiently at mid-temperatures but diminished at higher sintering temperatures, thereby reducing its negative impact on strength.

The addition of $Fe_2O_3$ strongly influenced the crystallization pathway by promoting spinel (hercynite) formation, reducing brittle cristobalite content, and encouraging the development of pyroxene and minor magnetite phases. These changes suppressed the formation of glassy or amorphous phases and improved the overall crystallinity of the ceramsite. As sintering temperature increased, the presence of cristobalite and fayalite diminished, while stable crystalline structures such as mullite and hercynite dominated, leading to a more thermally stable and mechanically robust matrix.

A strong correlation was observed between phase composition and compressive strength. At 1150°C, incomplete sintering and the presence of weak phases resulted in low strength. As the temperature rose to 1175°C and 1200°C, the formation of hercynite and pyroxene improved strength moderately. Optimal phase development occurred between 1275°C and 1300°C, where fayalite was nearly absent and mullite and hercynite peaked, resulting in the highest compressive strength. This confirms that 5 wt% $Fe_2O_3$ acts as a sintering aid and crystallization promoter, significantly enhancing the performance of CFB fly ash-based ceramsite.

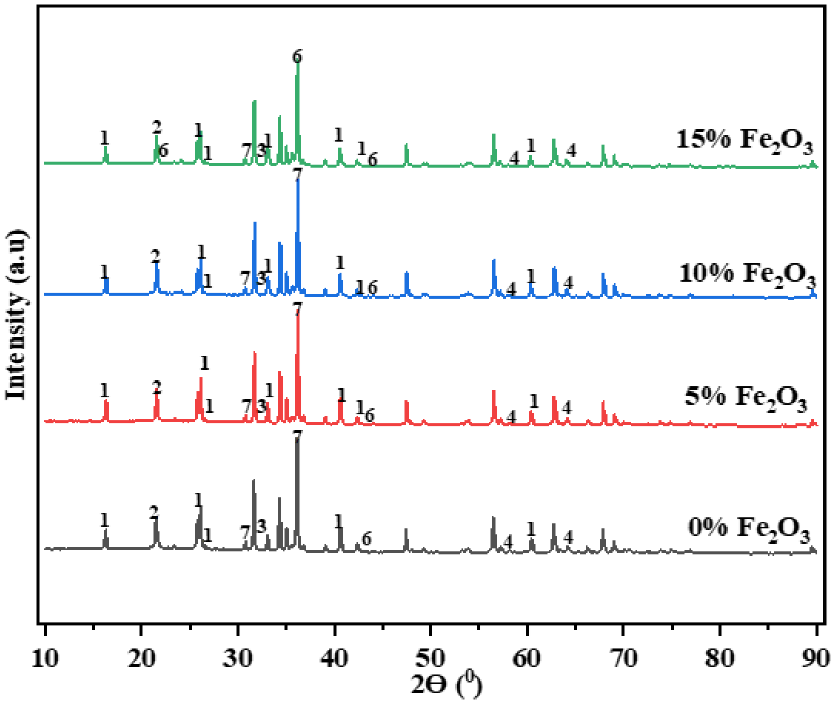

*Fig. 8. XRD analysis of ceramsite produced at 1300°C with varying ratios of $Fe_2O_3$ addition*

1-Mullite ($3Al_2O_3{\cdot}2SiO_2$); 2- Cristobalite ($SiO_2$); 3-Pyroxene $Ca(Mg,Fe)Si_2O_6$, 4-Magnetite ($Fe_3O_4$); 5-Anorthite ($CaAl_2Si_2O_8$); 6 Fayalite ($Fe_2SiO_4$); 7-Hercynite ($FeAl_2O_4$)

The XRD data, as illustrated in Eqs. (6), (7), (8), and (9), demonstrated that $Fe_2O_3$ played a crucial role in the formation of key mineral phases, including mullite, cristobalite, pyroxene, magnetite, fayalite, and hercynite, at different sintering temperatures. The mullite phase developed more rapidly as temperature increased (Eq. (6)), while the presence of $Fe_2O_3$ actively promoted the formation of hercynite, a mineral that enhanced liquid-phase sintering. This process contributed to the development of a dense, hercynite-rich network, which reinforced the silicate matrix, lowered porosity, and improved the compactness of ceramsite, ultimately leading to higher compressive strength [48].

However, when $Fe_2O_3$ content was increased further, the fayalite peaks became more prominent. The excess $Fe_2O_3$ negatively affected the stability of the crystal structure, causing over-melting and an increase in brittleness [40], which weakened the material's compressive strength. These mineral phase transformations during ceramsite sintering are described by the reactions in Eqs. (6), (7), (8), (9). (10) and (11).

$$3Al_2O_3 + 2SiO_2 \rightarrow 3Al_2O_3{\cdot}2SiO_2 \quad (6)$$

$$CaO + Al_2O_4 + 2SiO_2 \rightarrow CaAl_2Si_2O_8 \quad (7)$$

$$Fe_2O_3 + SiO_2 \rightarrow Fe_2SiO_4 \quad (8)$$

$$Fe_2O_3 + Al_2O_3 \rightarrow FeAl_2O_4 \quad (9)$$

Formation of pyroxenes (diopside and hedenbergite)

$$CaO+MgO+2SiO_2 \rightarrow CaMgSi_2O_6 \quad (10)$$

$$CaO+FeO+2SiO_2 \rightarrow CaFeSi_2O_6 \quad (11)$$

### 3.6 TG-DSC-FTIR Analysis

To examine weight loss dynamics and heat transfer mechanisms during ceramsite sintering, a thermogravimetric-differential scanning calorimetry (TG-DSC) analysis was conducted on CFB fly ash with $Fe_2O_3$ additions of 5 wt%, 10 wt%, and 15 wt% in an air atmosphere. As depicted in Fig. 8, the weight loss behavior of the four raw material samples follows a pattern that can be divided into three distinct phases, corresponding to substance volatilization at varying temperatures. The CFB fly ash sample's thermal reactions are highlighted in Fig. 8a, showing a total weight loss of approximately 3.74%, as evidenced by the TG curve, with noticeable weight loss phases occurring at different temperature ranges.

The initial weight loss phase, lasting approximately 100 minutes, results from the evaporation of free water, the breakdown of crystalline water, and minor desorption. As per Eq. (10), further weight loss beyond 160 minutes can be attributed to the thermal decomposition of $Ca(OH)_2$ and $CaCO_3$ in CFB fly ash. Subsequently, at 190 minutes, the material undergoes carbon combustion and additional $CaCO_3$ decomposition, as illustrated in Eq. (11). These transformations align well with the thermal events recorded in the DSC curve.

$$Ca(OH)_{2(s)} \rightarrow CaO_{(s)} + H_2O_{(g)} \quad (10)$$

$$CaCO_3 \rightarrow CaO_{(s)} + CO_{2\,(g)} \quad (11)$$

The weight loss behavior shown in Figures 8(b)–(d) follows a trend similar to that of CFB fly ash. A first endothermic peak appears between 100°C and 200°C, attributed to dehydration, which becomes more pronounced with increasing $Fe_2O_3$ content. Between 250°C and 400°C, a second endothermic peak suggests processes like carbon oxidation or the decomposition of carbonates. An important exothermic peak emerges between 600°C and 900°C, which is linked to the crystallization and development of silicate phases, such as calcium silicate and mullite, along with iron-containing phases like ferrite and hematite [26]. A smaller exothermic peak around 1000°C to 1200°C likely indicates the transition of iron-rich phases. For the sample with 5 wt.% $Fe_2O_3$, an additional exothermic peak above 1200°C was observed, marking the occurrence of high-temperature sintering.

Using TG-DSC-FTIR analysis, the thermochemical behaviour of CFB fly ash and the formation of gas phases during ceramsite sintering were investigated. Results from CFB fly ash samples with varying $FeO_3$ additions (0–15%) show important findings into the evolution of $CO_2$ and thermochemical reactions. The infrared absorption peaks associated with $CO_2$ were predominantly detected in the wavelength range of 2300–2400 $cm^{-1}$. This is correlated with carbonate decomposition or organic oxidation, with the intensity and position varying significantly with the $Fe_2O_3$ content and temperature. Compared with undoped ash, higher $Fe_2O_3$ concentrations (5–15%) attenuate the peak intensity (Fig. 9a–d), suggesting that $Fe_2O_3$ suppresses $CO_2$ generation by stabilizing carbon phases or promoting redox reactions that limit carbonate breakdown. The temperature-dependent behavior further shows that $CO_2$ release occurs in stages: minor peaks below 600°C correspond to labile carbonates, whereas stronger peaks at higher temperatures arise from refractory carbonates or silicate-bound $CO_3^{2-}$. The $Fe_2O_3$-doped samples exhibit delayed or broadened peaks, indicating the altered thermal stability of the carbonaceous components. This moderate gas release may increase the sintering kinetics by reducing pore formation, thereby increasing the ceramsite density.

The interaction between $Fe_2O_3$ and fly ash involves both physical and chemical mechanisms. $Fe_2O_3$ acts as a flux, lowering silicate melting points to promote liquid-phase sintering, which encapsulates carbonates and delays decomposition, minimizing abrupt $CO_2$ release. Additionally, $Fe^{3+}$ facilitates redox reactions, oxidizing residual carbon or sulfur compounds into non-gaseous intermediates and indirectly suppressing $CO_2$. The optimal $Fe_2O_3$ content at a ratio of 5 wt% to 10 wt% balances gas management and sintering efficiency, yielding ceramsite with reduced porosity and enhanced mechanical strength. These findings highlights the dual role of $Fe_2O_3$ in modulating reaction pathways and microstructural development, offering a strategic approach to optimize industrial waste valorization processes while aligning with sustainability goals through controlled gas emissions.

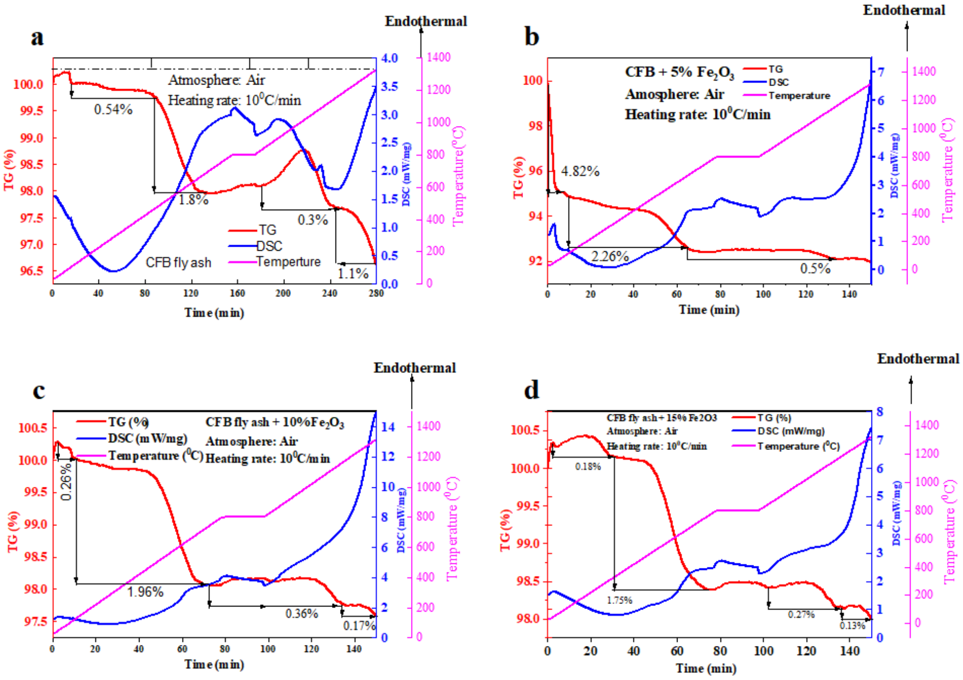

*Fig. 9 Thermal analysis TG-DSC curves of CFB fly ash with different $Fe_2O_3$ addition*

(a) CFB+0 wt% $Fe_2O_3$; (b) CFB+ 5 wt% $Fe_2O_3$; (c) CFB + 10 wt% $Fe_2O_3$; and (d) CFB+ 15 wt% $Fe_2O_3$

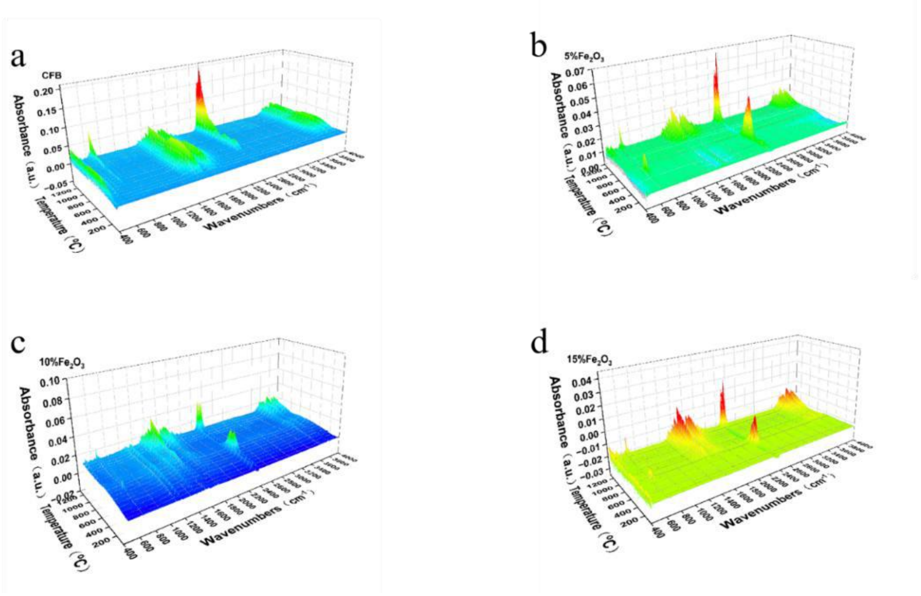

*Fig. 10. FTIR analysis of CFB fly ash across a range of temperatures*

(a) CFB + 0 wt% $Fe_2O_3$; (b) CFB + 5wt% $Fe_2O_3$; (c) CFB + 10wt% $Fe_2O_3$ and (d) CFB + 15wt% $Fe_2O_3$

## 3.7 Sintering mechanism of high-strength ceramsite

High-strength ceramsite made from circulating fluidized bed (CFB) fly ash is sintered through an intricate process of thermal, chemical, and microstructural changes, with the addition of $Fe_2O_3$ having a particularly significant impact. Sintering begins as a thermally induced process that causes densification, phase changes, and particle rearrangement [43], [46]. Three main phases make up the sintering process for ceramsite: initial neck development between particles, middle densification marked by pore contraction, and final grain growth, in which liquid-phase creation is important. $Fe_2O_3$, which functions as a fluxing agent, greatly improves the sintering process. In order to create low-melting-point eutectics like hercynite ($FeAl_2O_4$), $Fe_2O_3$ reacts with alumina ($Al_2O_3$) to lower the sintering temperature. Through viscous flow and grain boundary diffusion, these phases encourage the formation of a temporary liquid phase, which improves mass transport and makes particle rearrangement easier. As a result, there is less porosity, better particle bonding, and greater structural integrity [49].

In particular, the liquid-phase sintering process is optimized at moderate $Fe_2O_3$ concentrations (5 – 10 wt%). The liquid phase creates a dense microstructure with smaller pores, fills in interstitial spaces, and promotes the growth of crystalline phases, particularly mullite. A compact matrix and enhanced interparticle adhesion are revealed by SEM examination at this composition. Furthermore, $Fe_2O_3$ stabilizes carbon phases, moderates gas release, and delay thermal breakdown, all of which stop pore coarsening and bubble formation, according to FTIR and TG-DSC-FTIR investigations. However, excessive $Fe_2O_3$ additions (>10 wt%) result in over-fluxing, leading to excessive liquid-phase formation. This disrupts the balance between densification and bloating, increasing porosity due to uncontrolled gas release and the formation of large pores and microcracks. These structural defects reduce compressive strength and compromise the integrity of the ceramsite. According to morphological investigations, sintering at lower temperatures (1150–1175°C) produces poor densification and insufficient liquid-phase development. On the other hand, maximum shrinkage, improved densification, and minimal porosity are obtained by sintering at 1300°C with an ideal $Fe_2O_3$ concentration, suggesting a dominant liquid-phase sintering mechanism.

In conclusion, temperature-dependent phase transitions and the fluxing behaviour of $Fe_2O_3$ control the sintering mechanism of high-strength ceramsite. Through regulated liquid-phase sintering, a dense microstructure and stable crystalline phases are encouraged by an optimum $Fe_2O_3$ concentration. Achieving higher structural qualities and promoting the sustainable use of CFB fly ash in high-performance building materials depend on this mechanism.

### 3.8 Microscopic morphology analysis on compressive strength

Figure 11 shows the SEM analysis of ceramsite sintered at 1150°C and 1300°C, with $Fe_2O_3$ concentrations of 0 wt% and 5 wt%. The microstructure reveals how both sintering temperature and $Fe_2O_3$ influence the ceramsite's shape and density. The CFB fly ash sample fired at 1150°C (Figure 11a) has a rough, porous surface with little densification, which suggests that sintering was incomplete. When 5 wt.% $Fe_2O_3$ is added (Figure 11b), the pores become closed and better connected, showing some improvement in densification. This suggests that $Fe_2O_3$ may be acting as a flux, helping the sintering process begin. However, the overall porosity is still high, indicating that 1150°C is not enough to fully vitrify the material and improve its strength. The irregular pores and limited liquid-phase formation prevented the ceramsite from achieving the necessary compressive strength, as required by the Chinese National Standard. Thus, lower sintering temperatures do not result in the creation of high-strength ceramsite.

When the sintering temperature was increased to 1300°C, there was a clear improvement in the densification of the ceramsite. The CFB fly ash sample without $Fe_2O_3$ (Figure 11c) showed much less porosity, though a small crack remained, likely due to shrinkage or too much heat. The central cross-section of the ceramsite appeared smoother, with fine fractures between 10 and 40 µm and small connected pores of 5 to 10 µm in size. The higher temperature caused the CFB fly ash particles to melt, forming a liquid phase that flattened some of the sintered surfaces. However, the liquid phase at this stage was not enough to fill all the internal pores of the ceramsite. As a result, after cooling, the ceramsite had many communication pores, due to the interaction between gas and liquid phases.

At 1300°C, the 5 wt.% $Fe_2O_3$-modified sample showed excellent sintering behavior, with better densification and much lower porosity, as seen in Figure 11d. The liquid phase formed by the reaction of $Fe_2O_3$ at high temperatures played an important role in improving the ceramsite’s densification and reducing its porosity, which ultimately enhanced its compressive strength. This liquid phase development also helped to minimize the small amount of gas produced during sintering, further boosting the ceramsite's strength [27].

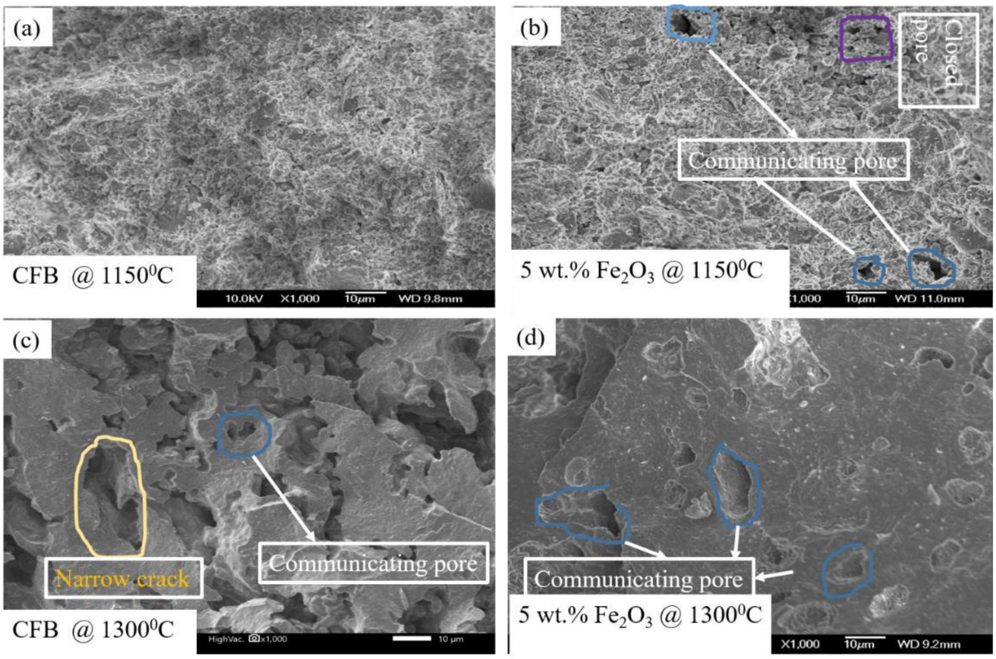

*Fig. 11. Scanning electron microscopy (SEM) images showing the effect of $Fe_2O_3$ additive on the ceramsite at different sintering temperatures with 0 - 5wt% $Fe_2O_3$ addition*

(a) CFB @ $1150^0$C; (b) 5wt.% $Fe_2O_3$ @ $1150^0$C; (c) CFB @ $1300^0$C; (d) 5wt.% $Fe_2O_3$ @ $1300^0$C

At 1200°C with 5 wt.% $Fe_2O_3$ (Fig. 12a), the microstructure is highly porous with disordered particle distribution, revealing poor sintering and weak interparticle bonding. The prevalence of micro-cracks and pores certifies that the material has not reached densification, and this could be detrimental to its mechanical strength and durability. This partial sintering is because of insufficient thermal energy to produce efficient diffusion and bonding among the particles. The material shows less porosity and better particle bonding as the temperature rises to 1250°C (Fig. 12b). The smoother surfaces indicate that liquid-phase sintering has begun, which improves densification. Even still, there are still some residual voids, suggesting that although the material is getting denser, full densification has not yet been reached.

The microstructure becomes noticeably denser at 1300°C with 5 wt% $Fe_2O_3$ (Fig. 12c), showing a clear sign of material aggregation and fewer visible pores. This implies that the sintering process has advanced to a point where improved particle rearrangement and densification are possible due to adequate liquid-phase formation. At this point, a glassy phase may emerge, which could increase the material's mechanical strength and resistance to external forces.

However, the microstructure displays bigger interconnected pores when the $Fe_2O_3$ content is raised to 10 wt% at the same temperature (Fig. 12d). This might be because of too much liquid-phase formation, which causes gas release or bloating during sintering. Grain boundary cracks provide additional evidence that the material's structural integrity may have been compromised by high temperatures. However, higher temperatures generally improve sintering and decrease porosity up to a certain degree, but too much $Fe_2O_3$ at high temperatures might have negative impacts like bloating. 5 wt% $Fe_2O_3$ at 1300°C is the optimum ratio for producing a high-strength ceramsite, where sintering is well-developed without having too much porosity.

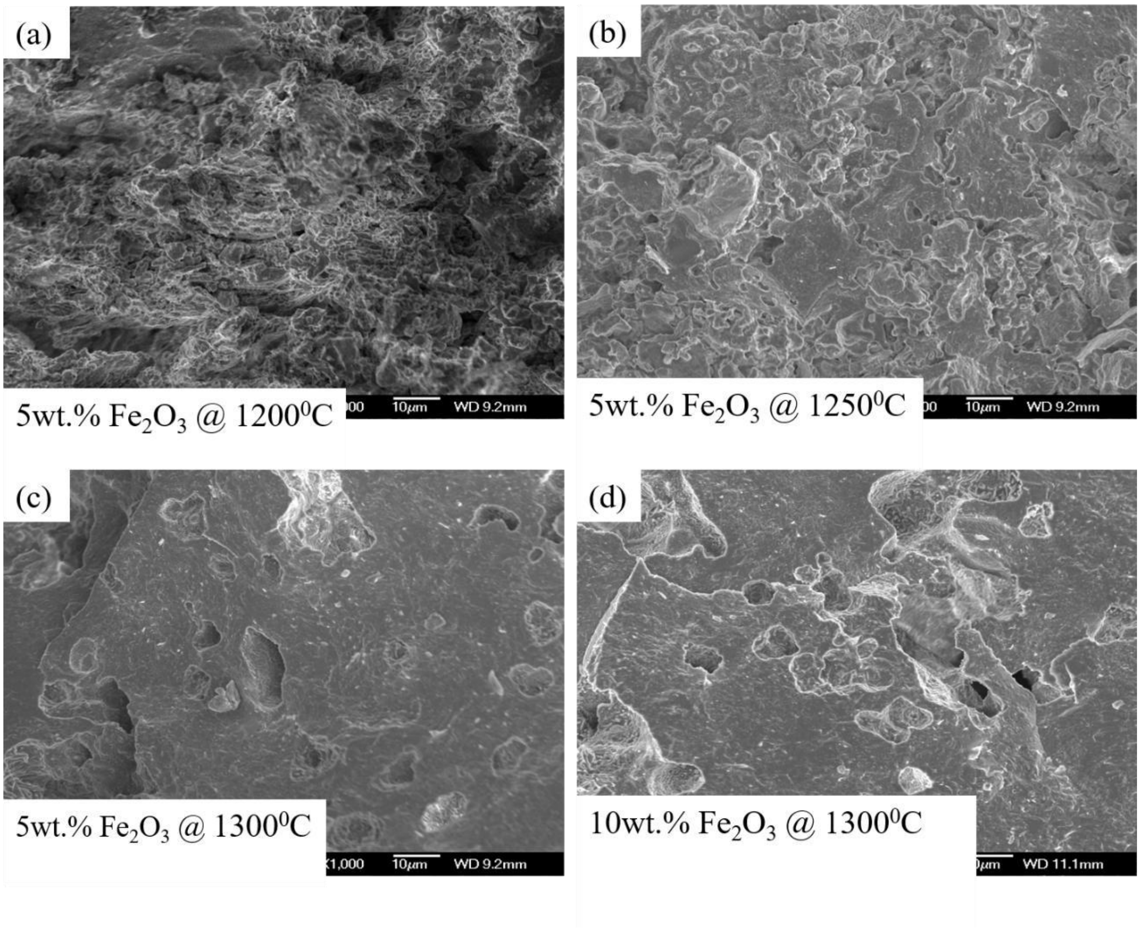

*Fig. 12. Scanning electron microscopy (SEM) of ceramsite at varying sintering temperatures with 5 wt% - 10 wt% $Fe_2O_3$ addition*

(a) 5wt.% $Fe_2O_3$ @ $1200^0$C; (b) 5wt.% $Fe_2O_3$ @ $1250^0$C; (c) 5wt.% $Fe_2O_3$ @ $1300^0$C; (d) 10wt.% $Fe_2O_3$ @ $1300^0$C

## IV. CONCLUSION

This study revealed that adding $Fe_2O_3$ in a controlled manner greatly improves both the sintering properties and the mechanical performance of ceramsite made from CFB fly ash. Under the best conditions, which involved adding 5 wt% $Fe_2O_3$ and sintering at 1300°C, the ceramsite achieved a compressive strength of 36.09 MPa, which is significantly higher than the 16.38 MPa observed in samples without $Fe_2O_3$. Water absorption also dropped dramatically, from 12.20% at 1225°C to only 0.19% at 1300°C, while both the apparent and stacking densities increased, rising from 1770.23 kg/m$^3$ to 2327.85 kg/m$^3$ and from 863.94 kg/m$^3$ to 1189.3 kg/m$^3$, respectively. The XRD and SEM analyses showed that $Fe_2O_3$ promoted the formation of a mullite-rich matrix and improved liquid-phase sintering, which enhanced particle bonding and created a more uniform pore structure. The shrinkage at 1300°C with 5 wt% $Fe_2O_3$ was around −15.58%, contributing to superior densification. However, when the $Fe_2O_3$ content was increased beyond 5 wt%, overfluxing occurred, which reduced the liquid phase viscosity, leading to a slight decrease in compressive strength and densification. Overall, these findings confirm that the controlled addition of $Fe_2O_3$ improves ceramsite's microstructure and performance, offering a sustainable approach for turning industrial waste into high-strength construction materials.

## DECLARATION OF AUTHORSHIP AND CONTRIBUTIONS

Ikechukwu Okeke and Peng Liyang contributed equally to the experimental design, data interpretation, and manuscript writing. Chibuike Chiemelie and Paul Afreh assisted in material preparation and lab analysis. Mahwish Islam contributed to data validation and editing. Prof. Qin Yuhong supervised the project and approved the final manuscript.

## DECLARATION OF COMPETING INTEREST

The authors state that they have no competing financial interests or personal relationships that may have influenced the findings in this paper.

## REFERENCES

[1] W. Zhang, S. Wang, J. Ran, H. Lin, W. Kang, and J. Zhu, "Research progress on the performance of circulating fluidized bed combustion ash and its utilization in China," *Journal of Building Engineering*, vol. 52, p. 104350, 2022.

[2] X. Chen, J. Gao, Y. Yan, and Y. Liu, "Investigation of expansion properties of cement paste with circulating fluidized bed fly ash," *Construction and Building Materials*, vol. 157, pp. 1154–1162, Dec. 2017, doi: 10.1016/j.conbuildmat.2017.08.159.

[3] R. Siddique, "Use of municipal solid waste ash in concrete," *Resources, Conservation and Recycling*, vol. 55, no. 2, pp. 83–91, 2010.

[4] X. Shan, Z. Ma, Y. Guo, and F. Cheng, "Study on characteristics of circulating fluidized bed pulverized fuel ash with different particle sizes," *Coal Science and Technology*, vol. 46, no. 11, pp. 232–238, 2018.

[5] M. Ning, Z. Wang, J. Qian, and S. Tang, "Characteristics of fluidized bed coal combustion fly ash and slag and its adaptability with current standards," *Bulletin of the Chinese Ceramic Society*, vol. 38, no. 3, pp. 688–693, 2019.

[6] K. He, Z. Lu, J. Li, and K. Song, "Comparative study on properties of circulating fluidized bed combustion ash and slag," *Journal of Wuhan University of Technology*, vol. 36, no. 3, pp. 6–13, 2014.

[7] J.-S. QIAN, Z.-W. ZHANG, H.-W. ZHENG, and Z. WANG, "Study on the varieties and distribution of sulfur minerals in CFBC ash/slag," *Journal of China Coal Society*, vol. 38, no. 4, pp. 651–656, 2013.

[8] A. González, N. Moreno, R. Navia, and X. Querol, "Study of a Chilean petroleum coke fluidized bed combustion fly ash and its potential application in copper, lead and hexavalent chromium removal," *Fuel*, vol. 89, no. 10, pp. 3012–3021, 2010.

[9] D. Qiao, J. Qian, Q. Wang, Y. Dang, H. Zhang, and D. Zeng, "Utilization of sulfate-rich solid wastes in rural road construction in the Three Gorges Reservoir," *Resources, conservation and recycling*, vol. 54, no. 12, pp. 1368–1376, 2010.

[10] H.-A. Nguyen, T.-P. Chang, J.-Y. Shih, C.-T. Chen, and T.-D. Nguyen, "Influence of circulating fluidized bed combustion (CFBC) fly ash on properties of modified high volume low calcium fly ash (HVFA) cement paste," *Construction and Building Materials*, vol. 91, pp. 208–215, Aug. 2015, doi: 10.1016/j.conbuildmat.2015.05.075.

[11] T. Ji, D.-D. Zheng, X.-F. Chen, X.-J. Lin, and H.-C. Wu, "Effect of prewetting degree of ceramsite on the early-age autogenous shrinkage of lightweight aggregate concrete," *Construction and Building Materials*, vol. 98, pp. 102–111, Nov. 2015, doi: 10.1016/j.conbuildmat.2015.08.102.

[12] J. Qin, C. Cui, X. Cui, A. Hussain, and C. Yang, "Preparation and characterization of ceramsite from lime mud and coal fly ash," *Construction and Building Materials*, vol. 95, pp. 10–17, Oct. 2015, doi: 10.1016/j.conbuildmat.2015.07.106.

[13] J. Pei, X. Pan, Y. Qi, H. Yu, and G. Tu, "Preparation and characterization of ultra-lightweight ceramsite using non-expanded clay and waste sawdust," *Construction and Building Materials*, vol. 346, p. 128410, Sep. 2022, doi: 10.1016/j.conbuildmat.2022.128410.

[14] T. Yu, Z. Zhao, and J. Li, "Effect of sintering temperature and sintering additives on the properties of alumina ceramics fabricated by binder jetting," *Ceramics International*, vol. 49, no. 6, pp. 9948–9955, 2023.

[15] Y. Long *et al.*, "Preparation of High-strength ceramsite from municipal solid waste incineration fly ash and clay based on CaO-SiO2-Al2O3 system," *Construction and Building Materials*, vol. 368, p. 130492, Mar. 2023, doi: 10.1016/j.conbuildmat.2023.130492.

[16] T. Li, T. Sun, and D. Li, "Preparation, sintering behavior, and expansion performance of ceramsite filter media from dewatered sewage sludge, coal fly ash, and river sediment," *Journal of material cycles and waste management*, vol. 20, pp. 71–79, 2018.

[17] S. Hua, D. Wu, J. Wu, S. Li, G. Liu, and D. Pei, "Characterization of the physical chemistry properties of iron-tailing-based ceramsite," *Molecules*, vol. 28, no. 5, p. 2258, 2023.

[18] X. Wang, Y. Jin, Z. Wang, Y. Nie, Q. Huang, and Q. Wang, "Development of lightweight aggregate from dry sewage sludge and coal ash," *Waste management*, vol. 29, no. 4, pp. 1330–1335, 2009.

[19] Z. Yang, W. Song, J. Yang, L. Deng, Z. Cao, and M. Shi, "High-strength ceramsite made with sludge and low-quality fly ash," *Journal of materials in civil engineering*, vol. 25, no. 7, pp. 851–856, 2013.

[20] C. Ou *et al.*, "Removal of ammonia nitrogen and phosphorus by porous slow-release Ca2+ ceramsite prepared from industrial solid wastes," *Separation and Purification Technology*, vol. 304, p. 122366, Jan. 2023, doi: 10.1016/j.seppur.2022.122366.

[21] M. Liu, Z. Zhu, Z. Zhang, Y. Chu, B. Yuan, and Z. Wei, "Development of highly porous mullite whisker ceramic membranes for oil-in-water separation and resource utilization of coal gangue," *Separation and Purification Technology*, vol. 237, p. 116483, Apr. 2020, doi: 10.1016/j.seppur.2019.116483.

[22] General Administration of Quality Supervision, "Inspection and Quarantine of the People's Republic of China, China National Standardization Administration Committee, Lightweight Aggregates and its Test Methods—Part 1: Lightweight Aggregates," Standards Press of China, Beijing, 2010.

[23] China Association for Engineering Construction Standardization, "High Strength Lightweight Aggregate," Standards Press of China, Beijing, 2020.

[24] C. M. Riley, "Relation of chemical properties to the bloating of clays," *Journal of the American ceramic society*, vol. 34, no. 4, pp. 121–128, 1951.

[25] D. Lindberg, C. Molin, and M. Hupa, “Thermal treatment of solid residues from WtE units: A review,” *Waste Management*, vol. 37, pp. 82–94, Mar. 2015, doi: 10.1016/j.wasman.2014.12.009.

[26] X. Wu *et al.*, “Preparing high-strength ceramsite from ferronickel slag and municipal solid waste incineration fly ash,” *Ceramics International*, vol. 48, no. 23, Part A, pp. 34265–34272, Dec. 2022, doi: 10.1016/j.ceramint.2022.07.357.

[27] M. Liu, C. Wang, Y. Bai, and G. Xu, “Effects of sintering temperature on the characteristics of lightweight aggregate made from sewage sludge and river sediment,” *Journal of Alloys and Compounds*, vol. 748, pp. 522–527, Jun. 2018, doi: 10.1016/j.jallcom.2018.03.216.

[28] B. Ma, Y. Li, G. Liu, and D. Liang, “Preparation and properties of Al2O3–MgAl2O4 ceramic foams,” *Ceramics International*, vol. 41, no. 2, pp. 3237–3244, 2015.

[29] L. Wang *et al.*, “Red mud-enhanced magnesium phosphate cement for remediation of Pb and As contaminated soil,” *Journal of Hazardous Materials*, vol. 400, p. 123317, Dec. 2020, doi: 10.1016/j.jhazmat.2020.123317.

[30] Y. M. Wie, K. G. Lee, and K. H. Lee, “Chemical design of lightweight aggregate to prevent adhesion at bloating activation temperature,” *Taylor & Francis*, Apr. 2020, Accessed: Jun. 24, 2024. [Online]. Available: https://www.tandfonline.com/doi/abs/10.1080/21870764.2020.1725259

[31] J. Pei, X. Pan, Y. Qi, H. Yu, and G. Tu, “Preparation of ultra-lightweight ceramsite from red mud and immobilization of hazardous elements,” *Journal of Environmental Chemical Engineering*, vol. 10, no. 4, p. 108157, Aug. 2022, doi: 10.1016/j.jece.2022.108157.

[32] H. Mi, L. Yi, Q. Wu, J. Xia, and B. Zhang, “Preparation of high-strength ceramsite from red mud, fly ash, and bentonite,” *Ceramics International*, vol. 47, no. 13, pp. 18218–18229, Jul. 2021, doi: 10.1016/j.ceramint.2021.03.141.

[33] J. Zou, G. Xu, and G. Li, “Ceramsite obtained from water and wastewater sludge and its characteristics affected by Fe2O3, CaO, and MgO,” *Journal of Hazardous Materials*, vol. 165, no. 1–3, pp. 995–1001, 2009.

[34] S. China, “Lightweight Aggregates and its Test methods—Part 2: Test Methods for Lightweight Aggregates,” *China Architecture& Building Press: Beijing, China*, 2010.

[35] S. Yashima, Y. Kanda, and S. Sano, “Relationships between particle size and fracture energy or impact velocity required to fracture as estimated from single particle crushing,” *Powder Technology*, vol. 51, no. 3, pp. 277–282, Aug. 1987, doi: 10.1016/0032-5910(87)80030-X.

[36] Y. Li *et al.*, “Measurement and statistics of single pellet mechanical strength of differently shaped catalysts,” *Powder Technology*, vol. 113, no. 1, pp. 176–184, Nov. 2000, doi: 10.1016/S0032-5910(00)00231-X.

[37] H. Wu *et al.*, “Sintering-free preparation of porous ceramsite using low-temperature decomposing pore former and its sound-absorbing performance,” *Construction and Building Materials*, vol. 171, pp. 367–376, May 2018, doi: 10.1016/j.conbuildmat.2018.03.152.

[38] Y. Chen *et al.*, “Adsorption mechanism of lead ions on porous ceramsite prepared by co-combustion ash of sewage sludge and biomass,” *Science of The Total Environment*, vol. 702, p. 135017, Feb. 2020, doi: 10.1016/j.scitotenv.2019.135017.

[39] J. Wang *et al.*, “The role of residual char on ash flow behavior, Part 2: Effect of SiO2/Al2O3 on ash fusibility and carbothermal reaction,” *Fuel*, vol. 255, p. 115846, Nov. 2019, doi: 10.1016/j.fuel.2019.115846.

[40] G. R. Xu, J. L. Zou, and G. B. Li, “Ceramsite obtained from water and wastewater sludge and its characteristics affected by (Fe2O3 + CaO + MgO)/(SiO2 + Al2O3),” *Water Research*, vol. 43, no. 11, pp. 2885–2893, Jun. 2009, doi: 10.1016/j.watres.2009.03.046.

[41] “Scopus preview - Scopus - Document details - Mixing water treatment residual with excavation waste soil in brick and artificial aggregate making.” Accessed: Jan. 27, 2025. [Online]. Available: https://www.scopus.com/record/display.uri?eid=2-s2.0-13244291562&origin=inward&txGid=40582fb43045979fabb17471f6f37f9d

[42] X. Zhenhua, L. Jianguo, S. Minying, and Z. Zhifei, “Effect of temperature on sintering ceramisite with sewage sludge and sediment,” *Chinese Journal of Environmental Engineering*, vol. 7, no. 5, pp. 1894–1900, 2013.

[43] C. Vakifahmetoglu and L. Karacasulu, “Cold sintering of ceramics and glasses: A review,” *Current Opinion in Solid State and Materials Science*, vol. 24, no. 1, p. 100807, Feb. 2020, doi: 10.1016/j.cossms.2020.100807.

[44] X. Wang *et al.*, “Revealing the intrinsic sintering mechanism of high-strength ceramsite from CFB fly ash: Focus on the role of CaO,” *Ceramics International*, Apr. 2024, doi: 10.1016/j.ceramint.2024.04.158.

[45] Y. Qin *et al.*, “Effect of biomass ash addition on coal ash fusion process under CO2 atmosphere,” *Fuel*, vol. 231, pp. 417–426, 2018.

[46]R. M. German, P. Suri, and S. J. Park, “Liquid phase sintering,” *Journal of materials science*, vol. 44, pp. 1–39, 2009.

[47] H. Wang, J. Xu, Y. Liu, and L. Sheng, “Preparation of ceramsite from municipal sludge and its application in water treatment: A review,” *Journal of Environmental Management*, vol. 287, p. 112374, Jun. 2021, doi: 10.1016/j.jenvman.2021.112374.

[48] L. Zhang *et al.*, “Investigation on coal ash fusibility and fluidity during the co-gasification of coal and coal indirect liquefaction residue,” *Fuel Processing Technology*, vol. 221, p. 106949, Oct. 2021, doi: 10.1016/j.fuproc.2021.106949.

[49] S.-M. Lee and S.-J. L. Kang, “Theoretical analysis of liquid-phase sintering: pore filling theory,” *Acta Materialia*, vol. 46, no. 9, pp. 3191–3202, 1998.